ACS POLYMERS Au
AN OPEN ACCESS JOURNAL OF THE AMERICAN CHEMICAL SOCIETY

pubs.acs.org/polymerau

Article

Photoinduced Electron Transfer and Changes in Surface Free Energy in Polythiophene-Polyviologen Bilayered Thin Films

Mary K. Danielson, Jie Chen, Anna K. Vaclavek, Nathan D. Colley, Abdul-Haq Alli, Richard A. Loomis, and Jonathan C. Barnes*

Cite This: *ACS Polym. Au* 2022, 2, 118−128

Read Online

ACCESS | Metrics & More | Article Recommendations | Supporting Information

ABSTRACT: Bipyridiniums, also known as viologens, are well-documented electron acceptors that are generally easy to synthesize on a large scale and reversibly cycle between three oxidation states (V^{2+}, $V^{\bullet+}$, and V^{0}). Accordingly, they have been explored in a number of applications that capitalize on their dynamic redox chemistry, such as redox-flow batteries and electrochromic devices. Viologens are also particularly useful in photoinduced electron transfer (PET) processes and therefore are of interest in photovoltaic applications that typically rely on electron-rich donors like polythiophene (PTh). However, the PET mechanism and relaxation dynamics between interfacing PTh and viologen-based thin films has not been well studied as a function of thickness of the acceptor layer. Here, a novel, bilayered thin film composite was fabricated by first spin-coating PTh onto glass slides, followed by spin-coating and curing polyviologen (PV)-based micron-sized films of variable thicknesses (0.5−11.3 μm) on top of the PTh layer. The electron-transfer mechanism and relaxation dynamics from the PTh sublayer into the upper PV film were investigated using femtosecond transient absorption (fTA) spectroscopy and electrochemistry to better understand how the charge-transfer/relaxation lifetimes could be extended using thicker PV acceptor films. The fTA experiments were performed under inert N_2 conditions as well as in ambient O_2. The latter shortened the lifetimes of the electrons in the PV layer, presumably due to O_2 triplet-based trap sites. Contact angle measurements using H_2O and MeI were also performed on top of the bilayered films to measure changes in surface free energy that would aid the assessment related to efficiency of the combined processes involving light penetration, photoexcitation, electron mobility, and relaxation from within the bilayered thin films. Insights gained from this work will support the development of future devices that employ viologen-based materials as an alternative electron-acceptor that is both easily processable and scalable.

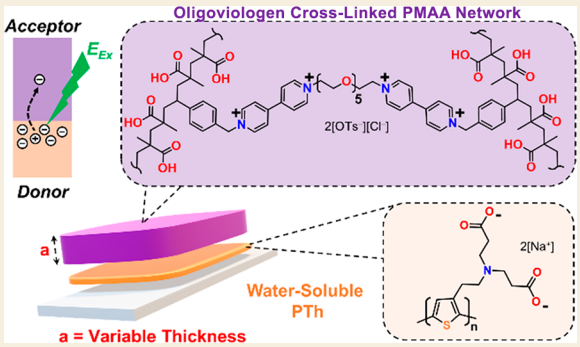

KEYWORDS: *polythiophene, polymethacrylic acid, polyviologens, photoinduced electron transfer, thin films, transient absorption spectroscopy*

INTRODUCTION

As the scientific community races toward "devices of the future," conducting polymeric materials and conjugated polymers have become important areas of study in chemistry and materials science.[1,2] At the center of these next-generation devices are donor−acceptor (D−A) pairs, used widely in the fabrication of organophotovoltaic (OPV)[3,4] and electrochromic devices.[5] While there is a vast library of known conjugated polymer donors and acceptors, only a few are utilized commercially. The limits placed on these D−A pairs are largely derived from a lack of visible-light absorption and low processability into films.

Perhaps some of the most popular donors for these devices are substituted polythiophenes like poly(3-hexyl thiophene),[6] commonly known as P3HT, although many others have been explored.[7,8] Yet, there is a noticeable lack of diversity among commercial acceptor compounds.[9] For example, most OPV materials rely on fullerene-derived acceptors[10,11] given their desirable electronic structures, while many electrochromic devices use doped tungsten oxides.[12] However, these acceptor materials can sometimes lack electronic tunability and are often tedious to synthesize. This has prompted an increased interest in developing novel acceptor compounds for their potential use in commercial applications.[9] For example, Sun et al.[13] recently synthesized in nine steps a brominated and conjugated acceptor compound with a zero HOMO offset between itself and a thiophene-based donor polymer. This combination resulted in

Received: September 22, 2021
Revised: November 19, 2021
Accepted: December 6, 2021
Published: December 22, 2021

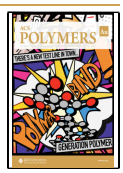

https://doi.org/10.1021/acspolymersau.1c00036
ACS Polym. Au 2022, 2, 118−128

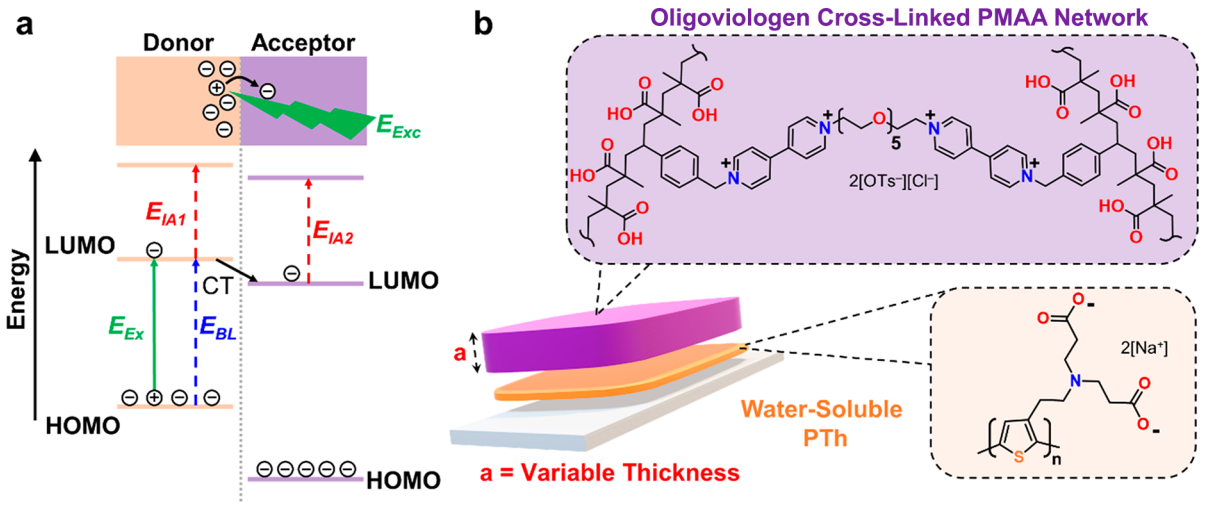

Figure 1. (a) General orbital energy diagram illustrating the mechanism of blue light-induced photoexcitation (E_{ex}) and electron transfer from a donor polythiophene (PTh) thin film to an acceptor oligoviologen cross-linked thin film of variable thickness (denoted as "a"). In studying this process, a bleach signal (E_{BL}) and an induced-absorption (E_{IA1}), both attributed to excitation within the donor layer were temporally characterized. A different induced-absorption absorption signal (E_{IA2}) is associated with the electron charge transfer (CT) into the acceptor layer, and it was also probed with time. (b) The bilayered thin films were fabricated from a water-soluble polythiophene and an oligoviologen cross-linked poly(methacrylic acid) (PMAA) with film thicknesses of 0.23 ± 0.03 μm and 0.5−11.3 μm, respectively.

one of the most highly efficient photovoltaic devices reported to date (photoconversion efficiency (PCE) of 16.32%).

Alternatively, simpler molecular designs that can be synthesized in fewer steps and on a larger scale are also of interest as potential electron-acceptor materials. One potential candidate is *N*,*N*′-dialkyl-4,4′-bipyridiniums (also known as viologens),[14,15] which are bipyridines that are readily alkylated at the nitrogen position, leading to dicationic moieties that can accept up to two electrons per viologen unit. Broad interest in bipyridinium salts stems from the ease with which their three reversible oxidation states can be accessed.[14,16] Specifically, the lower oxidation states ($V^{\bullet+}$ and V^0) are obtained through one- or two-electron reductions of the dication (V^{2+}), respectively. These well-documented reductions may be induced chemically,[17] electrochemically,[14] or photochemically.[18] Moreover, the dication (V^{2+}) is usually a pale-yellow color as its chloride salt, the radical cation ($V^{\bullet+}$) is dark purple, appearing almost black, and the diradical or neutral state (V^0) is reddish-orange as its chloride salt. These prominent redox-induced color changes make viologen-based materials ideal for electrochromic devices;[19−22] however, they have also been explored in supercapacitors,[23−25] redox-flow batteries,[26−29] and biological assays[30,31] and even as dopants in dye-sensitized solar cells[32,33] and quantum dots.[34,35]

Previously, we synthesized unimolecular and water-soluble oligo- and polyviologens with alternating main-chain backbones, where each viologen subunit was spaced on either side by oligoethylene glycol or hexamethylene subunits.[36−38] These well-defined viologen-based oligomers and polymers were used to cross-link polyacrylates to form homogeneous hydrogels that could reversibly contract and stiffen in response to chemical[38] or photoredox-based[36,39,40] reduction of the viologen subunits in the cross-linker. In the case of the photoredox-based mechanism, both tris(bipyridine) ruthenium(II) chloride ($[Ru(bpy)_3]Cl_2$) and a zinc tetraphenyl porphyrin (Zn-TPP) served as the electron donor upon photoexcitation with blue or blue/red light, respectively, and with triethanolamine functioning as a sacrificial reductant to regenerate each photocatalyst.

Since polythiophenes (PTh) and viologens were previously linked as useful D−A pairs in electrochromic applications,[41,19,42] we speculated that PTh could serve as a viable electron-transfer photocatalyst to reduce viologen-based polymers and related materials without the need for separate photocatalysts and sacrificial reductants. However, to simulate and better understand the nature and dynamics of electron transfer between a PTh donor and viologen-based acceptor within the context of a device setup, we aimed to fabricate layered D−A thin films that would allow for sufficient light penetration as a function of film thickness. Here, we describe a systematic investigation into the photoinduced electron transfer (PET) mechanism at play in novel PTh-viologen bilayered thin films (Figure 1) using femtosecond transient absorption (fTA) spectroscopy and electrochemistry. The micrometer-thick films were prepared by spin-coating the polythiophene derivative onto glass slides, followed by spin-coating and curing varying thicknesses of a viologen cross-linked poly(methacrylic acid) (PMAA) film on top of the PTh sublayer. Additionally, contact angle measurements were performed on the bilayered films pre- and post-PET to evaluate the efficiency of light penetration and electron transfer through the series of bilayered thin films. We envision that the PET mechanism and dynamics of the PTh-viologen thin-film composites reported here will serve as the basis on which new devices may be fabricated using viologen-based acceptor materials.

RESULTS AND DISCUSSION

Synthesis and Characterization

Poly(3,3′-((2-(thiophen-3-yl)ethyl)azanediyl)dipropionic acid) (PTh) used in this investigation was synthesized by following a previously reported method (see the Supporting Information (SI))[43] in which a thiophene-based propionate methyl ester precursor was treated with $FeCl_3$ to form the polymer, followed by saponification in strong base (NaOH) to generate the final anionic polymer. The negative charges helped facilitate solubility and processing in H_2O as well as electrostatic binding to the highly charged cationic PV-based film when the

https://doi.org/10.1021/acspolymersau.1c00036
ACS Polym. Au 2022, 2, 118−128

two materials were interfaced during fabrication. Also, the PTh used here was insoluble in nearly every solvent outside of H_2O, so effective bilayer film formation was easily achieved without dissolution of the donor sublayer. The PTh film was first prepared (Figure 2) in a 60 mg·mL^{-1} solution of 1:1 MeOH to

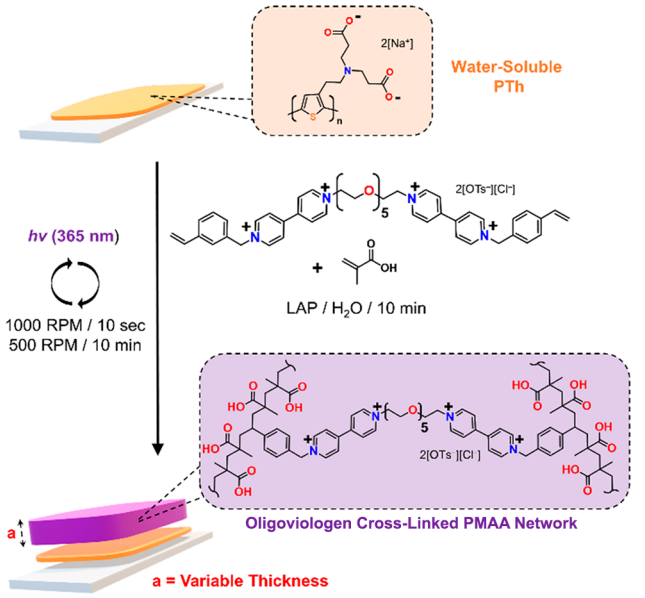

Figure 2. A 60 mg·mL^{-1} solution of PTh in 1:1 MeOH:H_2O was plated onto a 1″ × 1″ glass (borosilicate) microscope slide using a spin-coater. After drying, the PV/methacrylic acid mixture was polymerized photochemically while on the spin-coater directly on top of the PTh layer. The PV concentration and polymerization conditions were varied slightly dependent on the desired thickness of the acceptor PV film (oligoviologen cross-linked PMAA network).

H_2O. This solvent combination allowed for good solubility and a quick drying time. The solution was spin-coated onto a 1″ × 1″ glass (borosilicate) microscope slide and then quickly dried on a hot plate (60 °C) after spreading. The PTh layer appeared as a bright, transparent orange film after plating. The PV layer was subsequently polymerized on top of the dried PTh layer (vide infra). It is important to note that all syntheses were done in a class 100 cleanroom environment to prevent dust buildup between the two layers, as well as on top of the final bilayered film product.

The PV-cross-linked PMAA film, referred to herein as just "PV film" or "PV layer", was synthesized (Figure 2) from a methacrylic acid monomer and a 2V-St·2OTs·2Cl cross-linker. The prepolymer solution was spun on top of the PTh layer and polymerized in situ on the spin-coater by irradiating the slide with UV light (365 nm) as it was spinning. The pre-PV solution was prepared in an almost-neat combination of methacrylic acid and H_2O with the methacrylic acid monomer simultaneously functioning as the major solvent. The PV film color varied from light brown to a deep brown depending on the final thickness of the film. The bilayered film product was a glassy yet translucent brown color. The thickness of the bottom PTh layer was kept constant throughout the course of this study, while the top PV layer was varied between 0.5 and 11.3 μm.

The resultant bilayered film was uniform, as shown in the atomic force microscopy (AFM) images in Figure 3a; differences in thickness varied in the nanometer range from the surface of the films (Figures S15−S18). Similarly, optical

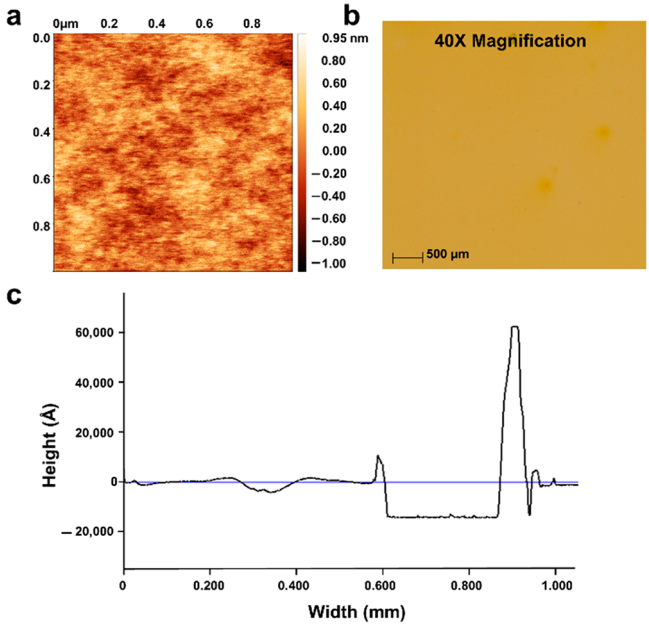

Figure 3. (a) AFM image of the surface of the 1.5 μm bilayered polymer film. Height differences of the film show fluctuations within a nanometer, indicating good uniformity. (b) Optical microscope image of the 1.5 μm bilayer polymer film at 40× magnification further confirms the uniformity of the surface and is consistent with the AFM data. (c) Profilometry data for the 1.5 μm bilayered polymer film confirmed the thickness of the two interfaced films by specifically measuring over an intentional scratch that was made in the films. A buildup in polymer on either side of the scratch produced the tall peaks.

microscopy was used (Figure 3b) to confirm visual uniformity at 40× magnification. The optical microscope images gave a good representation of the aforementioned color of the resultant films, a combination between the orange color associated with the PTh derivative and the brown color of the PV film. While characterizing the thickness of the film using profilometry (Figure 3c), further evidence of film uniformity was confirmed. The height or thickness of the film was determined by gently scratching through the bilayered films with a razor blade. This action resulted in a buildup of the soft, polymeric material at the edge of the scratch, but the remainder of the scan outside of the scratch location showed a uniform surface. The depth of the scratch, as measured with the profilometer, helped accurately quantify the total height of the film. Moreover, the uniformity of the films indicated an overall compatibility of the two films, PTh and PV, during the fabrication steps. Little to no determinable aggregation of polymeric material occurred in either film, even at very small thicknesses (Figures S7−S12).

Electrochemical Characterization

After the method was established for fabricating the bilayered films, the separated individual films (PTh and PV) were plated to study their solid-state electrochemical properties (Figure 4). Instead of the borosilicate microscope slides, both PTh and PV films were deposited via spin-coating onto conductive ITO slides. Notably, during cyclic voltammetry, the PV films showed reduction peaks on the first pass but failed to show oxidation peaks on the return pass. This is likely because the upper film is largely comprised of methacrylic acid and during the first sweep, the integrity of the film was disrupted. However, the discovery of the onset potentials for reduction and oxidation of each film (Figures S1 and S2) was crucial to understanding the electron

https://doi.org/10.1021/acspolymersau.1c00036
ACS Polym. Au 2022, 2, 118−128

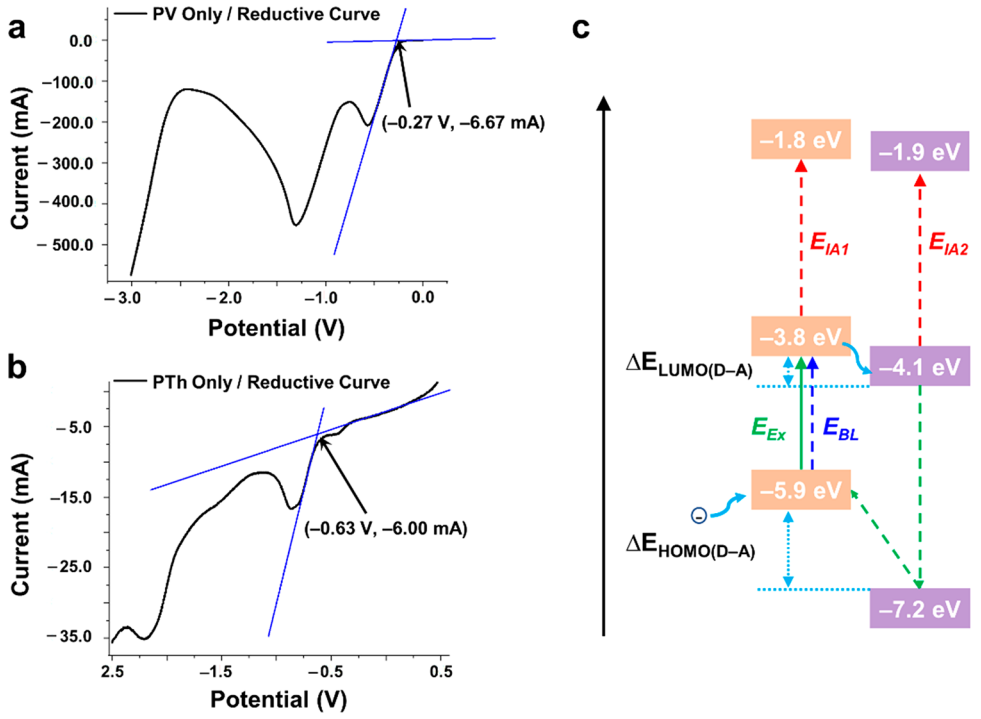

Figure 4. (a) Linear sweep voltammetry of a 1.5 μm PV cross-linked thin film on an ITO slide yielded onset peaks at 0.61 V for oxidation (Figure S2a) and −0.27 V for reduction. The latter information allowed for the calculation of the LUMO energy level associated with the PV film (−4.1 eV). (b) Linear sweep voltammetry of the PTh film on an ITO slide revealed onset peaks at 0.88 V for oxidation (Figure S1a) and −0.63 V for reduction. The latter potential resulted in a LUMO energy of −3.8 eV. (c) Corresponding orbital energy diagram with LUMO calculated from linear sweep voltammetry and HOMO from $E_{gap,optical}$ derived from UV−vis spectroscopy as well as higher energy orbitals determined from transient absorption spectroscopy data (vide infra). The small gap between the LUMOs of the two films indicates effective electron transfer upon excitation of the PTh is feasible.

transport mechanism. So, to protect the integrity of the films between scans, linear sweep voltammetry was used instead of cyclic voltammetry. The PV film showed onset potentials of 0.61 and −0.27 V for the oxidation and reduction, respectively, of the integrated viologen subunits (Figures S2a and 4a). Likewise, the PTh film showed onset potentials of 0.88 and −0.63 V for the oxidation and reduction, respectively (Figures S2b and 4b). These electrochemical experiments were conducted on films of thickness with 0.23 μm for the PTh film and 1.5 μm for the PV film and in the bilayered film (Figure S3). The measured reduction potentials allowed for the construction of part of the orbital energy diagram shown in Figure 4c, where the equation below was used to calculate the LUMO orbital energies using 4.4 eV as the value of IP(Fc), which refers to the internal standard redox potential of ferrocene:[44]

$$E_{LUMO} = - E'_{red,onset} - IP(Fc)\ eV$$

Canonically, for electron transfer to be effective enough for use in engineering applications, there needs to be a $\Delta E_{LUMO(D-A)}$ gap of around 0.3 eV between the donor and acceptor materials.[45] The two LUMO orbitals have energies of −3.8 and −4.1 eV for the PTh and PV layers, respectively, resulting in the requisite $\Delta E_{LUMO(D-A)}$ = 0.3 eV difference, supporting the claim that electron transfer is possible between the layered films. Additional information related to the HOMO energy values is included in the orbital energy diagram, which is based on data obtained from optical absorption spectroscopy and fTA experiments (vide infra).

UV−Vis NIR Absorption/Photoluminescence Spectroscopy Data

To initiate PET, the bilayered films need to be capable of absorbing enough light to photoexcite electrons in the PTh film and inject them into the upper PV film. Optical absorption spectroscopy (UV−vis-NIR) showed strong absorptions for both the PTh and PV films below 400 nm (>3.10 eV) (Figure 5a and b), thus making it unlikely that UV light could be used to selectively photoexcite the PTh film. However, the PTh film displayed a strong absorption from 400 to 600 nm (2.07 to 3.10 eV) that is largely lacking in the PV film absorption spectrum, thus representing an ideal wavelength range to induce electron transfer. A blue light source was therefore chosen in order to excite between 450−460 nm (~2.73 eV), allowing for absorption by the PTh film primarily, with minimal absorption by the PV film.

The individual films were plated onto microscope slides in the same manner as that for linear sweep voltammetry and were examined in the solid state. The onset values for the optical absorption peaks, i.e., $\lambda_{gap,optical}$ ($E_{gap,optical}$), were found at 593 nm (2.09 eV) for the PTh layer (Figure 5a) and 408 nm (3.04 eV) for the PV layer (Figure 5b).

The energy value of the HOMO could be discerned using the equation:[44]

$$E_{HOMO} = E_{LUMO} + E_{gap,optical}$$

Given this, the HOMO values were determined to be −5.9 and −7.2 eV for the PTh and PV layers, respectively. These values are consistent with reported values for both PTh- and PV-based

https://doi.org/10.1021/acspolymersau.1c00036
ACS Polym. Au 2022, 2, 118−128

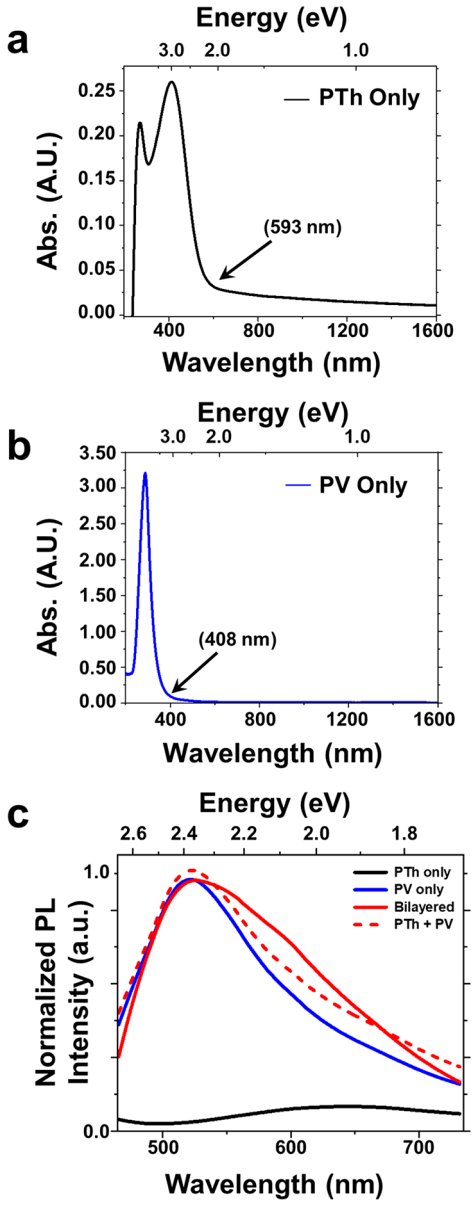

Figure 5. (a) UV−vis-NIR absorption spectrum of PTh only on a microscope slide. The onset of the absorbance was determined to be 593 nm (2.09 eV). (b) UV−vis-NIR absorption spectrum of PV only on a microscope slide. The onset of the absorbance was determined to be 408 nm (3.04 eV). (c) Photoluminescence (PL) spectra were recorded using excitation at 420 nm (2.95 eV). PL spectra of the samples are broad with maxima at 650 nm (~1.90 eV), 515 nm (2.41 eV), and 525 nm (~2.36 eV) for the PTh-only (black), PV-only (blue), and bilayer (red) films, respectively. The bilayered PL spectrum was fit to a sum of the PTh-only and PV-only PL spectra, which is shown as a dashed line. The relative contributions of the two PL spectra in the fit are illustrated by their relative intensities.

materials,[46,47] which allowed for the bottom portion of the orbital energy diagram in Figure 4c to be completed.

Photoluminescence (PL) experiments were performed (Figure 5c) on the PTh-only, PV-only, and bilayered films using excitation at 420 nm (2.95 eV). The PTh donor film has an absorption of 0.082 au at 420 nm, and the PL spectrum is broad with a maximum at near 650 nm (~1.90 eV). The PV acceptor film has a slightly lower absorption of 0.064 au at 420 nm, and the PL is broad with a maximum near 515 nm (2.41 eV). The PL spectrum of the bilayered films resembles the PV-only PL spectrum with a slightly shifted maximum at 525 nm (2.36 eV). In order to estimate the contributions from the PTh and PV layers in the bilayer PL spectrum, the bilayer PL spectrum was fit to a sum of the PL spectra of the two separate layers. The estimated contributions for each are indicated by the intensity scale used in Figure 5c. Thus, even though the absorption of the PTh layer is 28% greater than the absorption of the PV layer at 420 nm, the PL is dominated by the PV layer. Although the fitting of the shape of the bilayer PL spectrum is not ideal, these results strongly suggest the emission is predominantly from the acceptor PV layer, and there is charge transfer from the PTh layer to the PV layer following absorption.

Charge-Transfer Dynamics between the Donor and Acceptor Layers

The fTA experiments were performed (Figure 6a and b) to investigate the dynamics of the photoinduced charge transfer in the bilayered films. The absorption spectra of the PTh- and PV-only films served as a guide on how to best induce and probe the charge transfer from the PTh electron donor film to the PV acceptor layer. There is a small energy window near 500 nm (2.48 eV) where the top PV acceptor layer does not appreciably absorb, 0.027 au, but the bottom PTh layer does, 0.116 au. Consequently, most of the fTA experiments utilized excitation at 500 nm (E_{ex} = 2.48 eV). Even with this excitation wavelength, more signals than those from charge transfer are present in the fTA data collected for the bilayer samples, $\Delta\mathrm{Abs}(E, t)$; there are contributions from electronic excitation and relaxation within the separate layers. fTA experiments were therefore performed on thin-film samples containing just the bottom PTh electron-donor layer and just the top PV electron-acceptor layer, in addition to those performed on the PV/PTh bilayer, in order to identify and account for the contributions from each. All of the fTA data contain induced-absorption signals, $\Delta\mathrm{Abs}(E, t) > 0$, which are associated with new transitions not present in the unexcited samples. The fTA data also include bleach signals, $\Delta\mathrm{Abs}(E, t) < 0$, associated with decreases in transition probabilities caused by increases of the electron populations in excited levels or hole populations induced in HOMO levels caused by the excitation or pump pulse. In order to facilitate comparisons of the fTA data with the energies of the bands measured in the voltammetry experiments, from this point forward the energies instead of wavelengths of the fTA signals in the spectral data will be referenced.

The fTA data set acquired using E_{ex} = 2.48 eV on the sample containing only the bottom PTh layer is included in Figure 6a. This excitation immediately (within the temporal resolution of the measurements, ~200 fs) gave rise to a bleach signal, E_{BL}, or decreased absorption at the HOMO−LUMO gap of the PTh near 2.55 eV as electrons were promoted to the LUMO band and holes (or electron deficiencies) were generated in the HOMO band. These bleach signals (blue) in Figure 6a remained for as long as there were either electrons in the LUMO or holes in the HOMO band through the volume region of the sample probed. As will be mentioned, there is a bleach signal to higher energies associated with the PV acceptor layer and the temporal profiles were measured at 2.38 eV (520 nm) to avoid contributions from these signals. The temporal profile of the E_{BL} feature at 2.38 eV (Figure S27b in the SI, decays multiexponentially with an average decay lifetime of 740(80) ps. This excitation also resulted in a long-lived induced-absorption feature (red) near 1.72 eV associated with electronic transitions

https://doi.org/10.1021/acspolymersau.1c00036
ACS Polym. Au 2022, 2, 118−128

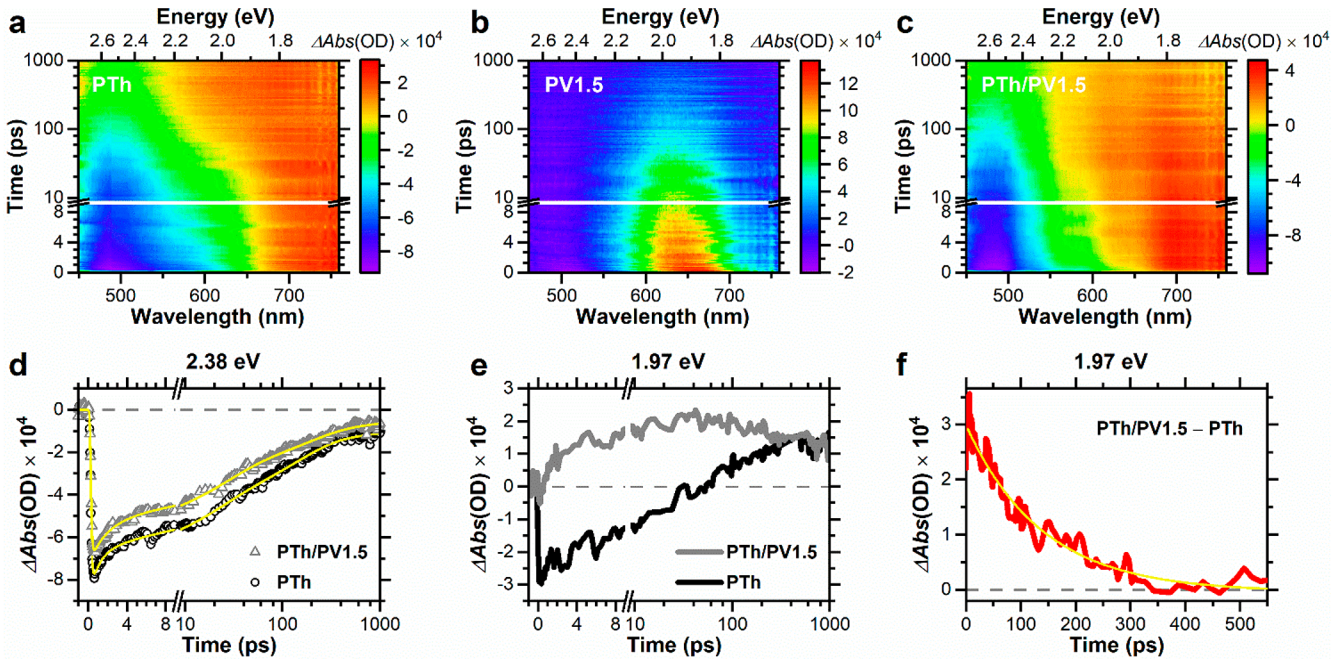

Figure 6. (a) Femtosecond transient absorption (fTA) data collected on the PTh bottom layer using E_{ex} = 2.48 eV. (b) fTA data collected on the PV1.5 top layer excited with E_{ex} = 2.76 eV. (c) fTA data of the PTh/PV1.5 bilayered film with E_{ex} = 2.48 eV. (d) Temporal profiles of the bleach signals from the PTh film, gray triangles, and the PTh/PV1.5 bilayer, black circles, measured at a probe energy of 2.38 eV in the data are included in (a) and (c), respectively. (e) Temporal profiles of the PTh bottom layer (black) and the PTh/PV1.5 bilayer (gray), measured at a probe energy of 1.97 eV in (a) and (c), respectively. (f) Temporal profile of the electron occupancy in the PV1.5 layer associated with charge transfer from the PTh layer (red curve) was estimated by subtracting the PTh signal from the PTh/PV1.5 signal probed at 1.97 eV in (a) and (c), respectively. The fit of this profile to a single-exponential decay is shown (yellow).

out of the LUMO state of the excited PTh film, indicated by E_{IA1} in the schematic in Figure 4c. The temporal profile of this signal is included in Figure S26. An accurate determination of the lifetime for this signal (>1 ns) is not possible with the current fTA apparatus due to the lifetime being longer than can be measured with the apparatus. The shorter decay lifetime of the E_{BL} signal (2.38 eV) in comparison to that of the E_{IA1} signal (1.72 eV) is attributed to the filling of the electron vacancies (or holes) in the HOMO of the PTh layer with electrons originating from outside the excitation volume in this layer or from the salts in the PTh layer.

The goal in these experiments was to identify and characterize the photoinduced electron transfer from the PTh later to the PV layer. Thus, it was necessary to characterize the transient signals associated with electrons in the electron-acceptor PV layer. To do so, separate fTA experiments were performed on PV-only layer samples. As mentioned, there is weak absorbance of the PV layer at E_{ex} = 2.48 eV (500 nm) (Figure 5b) and no measurable fTA signals were obtained using this pump photon energy (Figure S28). Consequently, experiments were performed on the PV-only films with E_{ex} = 2.76 eV (~450 nm), just at the turn-on of the absorption. The fTA data for the PV1.5 film sample recorded using E_{ex} = 2.76 eV are included in Figure 6b. There is an immediate bleach signal present at high energies, not shown, that is associated with excitation of the PV. There is also a prominent induced-absorption signal near 1.97 eV associated with the presence of electrons in an excited state of the PV. This transition is identified as E_{IA2} in Figure 4c. This E_{IA2} signal was used to track the PTh to PV layer charge transfer.

The fTA data collected on the PTh/PV1.5 bilayer sample is included in Figure 6c, and cursory inspection indicates these fTA data contain similar bleach and induced-absorption signals as present in the PTh-only top layer (Figure 6a). The fTA spectra associated with different delay times are plotted in Figure S30 to illustrate there are differences in the data for the PTh and PTh/PV1.5 samples. The multiexponential temporal profiles of the E_{BL} signals at a probe energy of 2.38 eV (520 nm) are included in Figure 6d. The average lifetime of this bleach feature is shorter for the bilayer sample than the PTh-only sample, 450(30) versus 760(80) ps (Table S2 in the SI). The shorter lifetime is associated with transfer of excited-state electrons from the PTh donor layer to the PV1.5 acceptor layer and the filling of holes in the PTh layer with either electrons transferred back from the PV layer or from the salts present in the PTh layer.

The temporal profile of the fTA data of the PTh/PV1.5 bilayer measured at the energy of the E_{IA2} signal associated with electrons transferred to the PV1.5 layer, 1.97 eV, is shown as gray in Figure 6e. This profile is markedly different from that measured at the same energy on the PTh data (black in Figure 6e), and these differences are attributed to the electrons in the PV1.5 layer. In order to extract the dynamics of the charge-transfer processes and subsequent relaxation of the electrons in the PV1.5 layer, the fTA data of the PTh-only sample was subtracted from the data collected of the PTh/PV1.5 bilayer sample. The two temporal profile at 1.97 eV is plotted in Figure 6f. This charge-transfer induced-absorption signal (red) appears with an instrument-limited rise time and decays with a single-exponential lifetime of 140(1) ps.

Additional fTA experiments were performed on the bilayer samples with thinner and thicker PV layers, PTh/PV0.5 and PTh/PV4, as well as the corresponding PV-only films to probe the impact of the thickness on the electron transfer and relaxation dynamics. The fTA data are presented in Figure S29, and they are qualitatively similar to the results included in Figure

https://doi.org/10.1021/acspolymersau.1c00036
ACS Polym. Au 2022, 2, 118−128

6c. The rise times of the E_{BL}, E_{IA1}, and E_{IA2} signals for all three samples are 100 fs or less, notably shorter than the instrument response, ~200 fs. The average decay lifetime of the E_{BL} signal at 2.38 eV is slightly smaller for the PTh/PV0.5 bilayer, 404(7) ps, than that measured for the PTh/PV1.5 bilayer, 450(30) ps (Table S1). The average lifetime of the E_{BL} signal is notably longer for the for the thicker PTh/PV1.5 bilayer, 740(80) ps. The temporal profiles of the E_{IA2} signals at 1.97 eV were estimated in the same manner as described above by subtracting the fTA data acquired for the PTh sample from the PTh/PV0.5 and PTh/PV4 bilayer samples (Figures S31 and S32). The single-exponential decay constant of the E_{IA2} temporal profile of the PTh/PV0.5 sample, 167(1) ps, is slightly longer than the profile of the PTh/PV1.5 sample, 140(1) ps. Note that the error indicated is from the fit and it is not from measuring the data from multiple bilayer samples. The lifetime of the E_{IA2} signal of the PTh/PV4 sample is notably longer, 204(1) ps.

It is possible contributions from carrier−carrier interactions or cumulative effects, such as the buildup of charge in the PTh layer, could be contributing to the observed dynamics and lifetimes in the fTA data. Additional fTA experiments were performed using 2.5× higher excitation fluences (Figure S33). The magnitude of the $\Delta Abs(E, t)$ signals increased with fluence, but they did so proportionally at all E and t. This suggests there are no or minimal carrier−carrier interactions contributing to the fTA data. To probe for charging or photoinduced changes in the bilayer samples, fTA data were continuously recorded over a 3 h period (Figure S34). The fTA data collected did not change with time, and they do not contain evidence for charging. Note that charging of the PV layer, perhaps temporarily, would likely result if it were not a salt.

The fTA experiments just described were performed with the samples maintained under a nitrogen atmosphere to minimize the presence of oxygen and the possible opening of triplet states that could trap electrons and contribute to the dynamics. Several fTA experiments were also performed on PTh/PV1.5 bilayer samples in air using E_{ex} = 2.48 eV to probe the impact of oxygen on the electron dynamics. The temporal profile of the E_{IA1} signal at 1.72 eV collected for the PTh/PV1.5 bilayer under air is the same within error as the profile collected for the PTh/PV1.5 sample in nitrogen (Figure S26). This suggests the charge-transfer from the excited PTh layer to the PV layer is not influenced by the presence of oxygen. The lifetime of the E_{IA2} signal at 1.97 eV is shorter with oxygen present, dropping from 140(1) to 106(1) ps. This shortening could be due to two factors. It is possible that the rate for transfer from the PV1.5 layer back to the PTh layer was enhanced with oxygen, but it is more likely there were trap sites present in the PV layer, such as triplet states, into which the electrons relaxed within the PV layer. Either of these competing pathways would have resulted in an increase of the total rate of electron loss in the PV layer. The temporal profile of the E_{BL} signal associated with excitation within the PTh layer at 2.38 eV is shorter with oxygen present (Figure S27); the average decay lifetime dropped from 450(30) ps in nitrogen to 237(5) ps with oxygen present. This change in E_{BL} lifetime indicates there is a significant contribution of the observed recovery dynamics in the PTh layer from the back transfer of the electrons from the PV layer to the PTh layer.

We propose the following mechanisms and charge carrier dynamics based on the fTA data. The photoexcitation with E_{ex} = 2.48 eV light promotes electrons in the PTh layer. A significant and measurable fraction of the excited electrons in the PTh layer, likely those in proximity to the PTh/PV interface, transfer to an excited state within the PV1.5 layer on ultrafast time scales. The evidence that only a fraction of the electrons transfer to the PV layer is the notably longer lifetime of the E_{IA1} signal, >1 ns, in comparison to the instrument-limited rise time of the E_{IA2} signal. The electrons transferred to the PV layer may diffuse throughout the layer, until they ultimately transfer back to the PTh layer. The longer lifetime of the E_{IA2} signal for the thicker PTh/PV4.0 bilayer in comparison to the thinner PTh/PV0.5 and PTh/PV1.5 bilayers suggest these electrons may sample distances longer than 1.5 μm into the PV acceptor layer. The temporal profiles of the bleach signals associated with excitation of the PTh layer have multiexponential decays associated with contributions from several mechanisms, including transfer of electrons from the PV layer back to the PTh layer, depopulation of electrons out of trap states, electron transfer from the salt, and relaxation of electrons in the PTh that do not transfer to the PV1.5 layer.

Droplet Contact Angle Experiment

After the photoluminescence and TA experiments showed effective electron transfer between the two layers, we became interested in measuring the change in surface energy as the top, PV layer's viologen subunits were reduced from a dicationic state (V^{2+}) to a monoradical cation ($V^{\bullet+}$). Since the cross-linking density was very high, the amount of viologen in the top layer was considerable. To investigate the change in surface energy as a function of the PV film's thickness, droplet contact angle experiments were conducted (Figure 7). We assumed there would be a smaller contact angle in a water-droplet experiment when the PV layer was oxidized (Figure 7a), and a

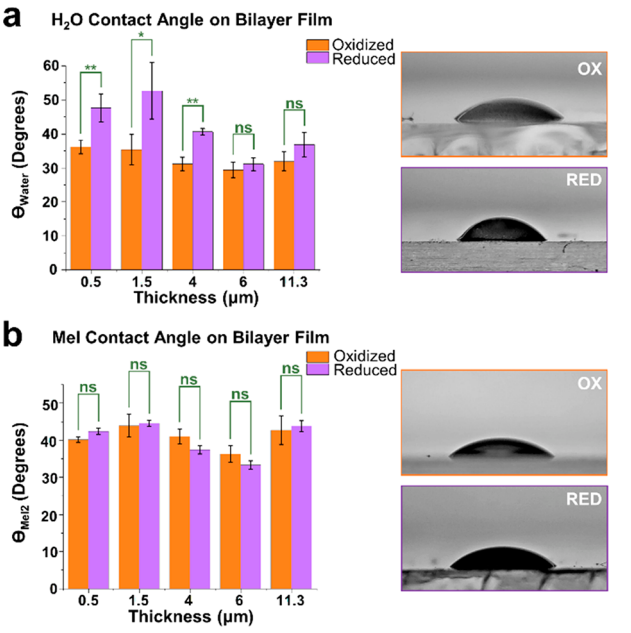

Figure 7. (a) Histogram showing average H_2O droplet contact angle at t = 1 s after dropping onto the bilayered film at varying thicknesses of the PV layer of the film. Statistically significant differences are noted at total thicknesses below 6 μm before and after reduction of the PV film. Images of the droplets at t = 1 s are shown on the right. Similar data is presented in (b) with MeI as the liquid, although no significant differences were noted in contact angle at any thickness. The corresponding images of the MeI droplets are shown to the right of the histogram. Note: $*p < 0.05$, $**p < 0.01$, ns = no statistical significance.

https://doi.org/10.1021/acspolymersau.1c00036
ACS Polym. Au 2022, 2, 118−128

larger contact angle when the PV layer was reduced on account of the corresponding charges and polarity. To test this theory, the bilayered film was irradiated with blue light to trigger electron transfer from the PTh to the PV layer. A secondary experiment was conducted (Figure 7b) with MeI, a compound with a neutral polarity. The droplet contact angle was expected to change between oxidation states of the viologen subunits in the PV film with H_2O and was not expected to change with addition of MeI.

The droplet experiments were conducted both before and after irradiation with blue light for 1 h. After compilation of the data, there was a notable difference between the H_2O droplets on the surface of the bilayered film before and after reduction at all thicknesses below 6 μm. This is significant because it supports a measurable, physical change occurring in the material in response to the collection and retention of electrons in the PV layer that originated from the photoexcited PTh layer. Interestingly, although not surprisingly, there was a marked drop-off in the effectiveness of the electron shuttling away from the films' interface at thicknesses larger than 4 μm. This was expected as the excited electrons have a finite lifetime and may encounter more trap sites in a thicker PV layer. If they could not be shuttled toward the surface of the bilayered film before that time, there would be no measurable change in the surface energy. Likewise, there was no significant difference between the MeI droplets before or after reduction. This is evidence that the interaction with the surface has to do with the change in polarity of the PV film. Any change due to heat or other experimental variables would have resulted in a consistent change in both droplet contact angle trials.

CONCLUSIONS

Seeking to better understand the mechanism and relaxation dynamics associated with electron transfer between a photoexcited donor PTh thin film that was directly interfaced with an acceptor PV thin film, we used solid-state electrochemistry and fTA to probe the excitation and charge transfer processes as a function of the acceptor film's thickness. In this systematic investigation, the PTh sublayer was set at ~0.23 μm thick, and the PV layer was varied from 0.5 up to 11.3 μm. It was shown that the thicker acceptor layers up to 4 μm were able to retain the injected electrons for longer periods of time before charge recombination occurred between the sublayer and upper PV film. Moreover, droplet contact angle experiments were performed by dropping either H_2O or MeI onto the surface of the bilayered thin films (i.e., on top of the PV film). A correlation between contact angle and film thickness was determined, whereby the samples with thicknesses greater than 4 μm did not exhibit any changes in surface free energy, as evidenced by a lack of change in the droplet curvature and relative angle. We envision the findings from this work will aid the development of future devices that employ viologen-based materials as an alternative electron-acceptor that is both easily processable and scalable.

METHODS

Materials

In this work, all reagents were purchase from commercial suppliers and used without further purification. 3-Thienylethanmine was prepared following a reported literature procedure.[48] Synthesis of dimethyl 3,3′-((2-(thiophen-3-yl)ethyl)azanediyl)dipropionate and poly(3,3′-((2-(thiophen-3-yl)ethyl)azanediyl)dipropionic acid) was conducted following a reported literature procedure.[43] The viologen cross-linker was synthesized following preparatory procedures from our previous work.[36,38] Films were fabricated using 1″ × 1″ cut sodium silicate microscope slides. TA measurements were performed in N_2 and in air using the output of a commercial Ti: sapphire amplifier laser system and a commercial TA spectrometer. Contact angle data was acquired using a Samsung Note 10+ camera with a Clarus 15× macro lens and all data was analyzed in ImageJ.

Synthesis of Poly(3,3′-((2-(thiophen-3-yl)ethyl)azanediyl)dipropionic Acid)

$FeCl_3$ (3.15 g, 19.47 mmol, equiv) was added to a 200 mL round-bottom flask and suspended in 50 mL of $CHCl_3$. Then, the mixture was allowed to stir at room temperature for 30 min. After 30 min, the monomer (1.46 g, 4.87 mmol, 1 equiv) was dissolved in 5 mL of $CHCl_3$ and added dropwise to the reaction flask. The reaction was allowed to stir at room temperature for 2 days. After this time, 10 mL of MeOH was added to the flask. A thick black oil precipitated out of the solution. The precipitate was collected and washed with 200 mL of a 1:1 mixture of $CHCl_3$:MeOH. The precipitate was then dissolved in 10 mL of DMSO and added to a small 50 mL round-bottom flask. Then 30 mL of 3 M aqueous NaOH solution was added to the flask. The reaction was heated to 50 °C and allowed to stir for 12 h. After 12 h, the reaction mixture was transferred to a dialysis bag (MW cutoff 1 kDa) and dialyzed for 2 days in deionized H_2O. The resulting product from the dialysis bag was filtered. The H_2O was evaporated to yield 3.12 g (99% by weight) of the water-soluble polythiophene. ^{1}H NMR (300 MHz, D_2O) δH 7.27 (s), 4.66 (s), 3.28 (s), 2.46 (s).

Since it was difficult to calculate the number-average molecular weight (M_n) of PTh from ^{1}H NMR (Figure S22), the retention time of the esterified PTh precursor was determined in DMF using gel permeation chromatography (GPC) and compared to water-soluble polyethylene glycol (PEG) standards (Figure S20). A calibration plot was constructed from the corresponding retention times of the PEG standards (Figure S21), from which M_p (the peak molecular weight) was extrapolated. This approach allowed us to calculate M_p = 10 800 g·mol^{-1} and a peak degree of polymerization (DP_p) equal to 36 subunits on average.

Synthesis of 2V-St·2OTs·2Cl: Styrene-Capped Dimer Cross-Linker

2V·2OTs (1.6 g, 1.8 mmol, 1 equiv) and 4-vinylbenzyl chloride (11.0 g, 72 mmol, 40 equiv) were dissolved in MeCN (dry, 40 mL, 40 mg/mL 2V·2OTs) and heated to 55 °C for 72 h. After 72 h, MeOH (10 mL) was added to the solution to dissolve the precipitate and the solution was transferred to four 50 mL centrifuge tubes and diluted with 40 mL of toluene (PhMe) to precipitate the product. The tubes were centrifuged at 4500 rpm at −10 °C for 30 min. The resulting supernatant was decanted, and the viscous, brown oil was washed by adding 50 mL of MeCN to each tube, followed by sonication and centrifugation. The supernatant was decanted, and this process was repeated three times. The oil was then dissolved in 5 mL of MeOH and precipitated a final time by adding 50 mL of 1:1 PhMe: Et_2O to yield 0.8 g (39%) of the desired product, 2V-St·2OTs·2Cl, as a dark brown, viscous solid. ^{1}H NMR (500 MHz, $(CD_3)_2SO$): δH 9.65 (d, J = 6.4 Hz, 4H); 9.40 (t, J = 8.5 Hz, 4H); 8.93−8.76 (m, 8H); 7.66 (d, J = 8.1 Hz, 4H); 7.55 (d, J = 8.1 Hz, 4H); 7.47 (d, J = 7.9 Hz, 4H); 7.08 (d, J = 7.8 Hz, 4H); 6.74 (dd, J = 17.6, 11.0 Hz, 2H); 6.02 (s, 4H); 5.91 (t, J = 16.4 Hz, 2H); 5.32 (d, J = 11.0 Hz,2H); 4.97−4.88 (m, 4H); 4.02−3.90 (m, 4H); 3.61−3.52 (m, 4H); 3.49−3.31 (m, 5H); 2.26 (s, 1H).

Polythiophene Bottom-Layer Film Fabrication

A 60 mg·mL^{-1} solution of polythiophene was made using a 1:1 mixture of MeOH and H_2O. To generate the bottom layer, the 1″ × 1″ glass slide was heated to 125 °C using a hot-plate. The hot slide was then quickly transferred to the spin-coater and 250 μL of the polythiophene mixture was deposited onto the slide. Spin conditions: 2 s at a velocity of 4500 rpm (ramp = 4500 rpm/s). After spinning, the slide was placed back on the hot plate for 30 s to ensure even drying.

Polyviologen (PV) Cross-Linked Top-Layer Film Fabrication (0.5−4 μm). An amount of 75 mg of 2V-St·2OTs·2Cl cross-linker was

https://doi.org/10.1021/acspolymersau.1c00036
ACS Polym. Au 2022, 2, 118−128

weighed and added into a 10 mL round-bottom flask. Then 1.25 mg of lithium phenyl-2,4,6-trimethylbenzoylphosphinate (LAP) was added to the reaction flask. Then, 225 μL of methacrylic acid and 75 μL of deionized H_2O were added to the reaction flask for the 0.5 and 1.5 μm films. For the 4 μm films, 257 μL of methacrylic acid and 43 μL of deionized H_2O were added to the reaction flask. The mixture was sonicated to ensure that all cross-linker and initiator were dissolved. Then, the mixture was degassed through freeze−pump−thawing three times. The mixture was then transferred into a clean room and plated on top of the polythiophene-coated substrate. Then 300 μL of the mixture was plated onto the polythiophene-coated substrate on a spin-coater. During the second spin step (10 min), the mixture and substrate were irradiated with a UV (365 nm) 75 W light source, positioned 3″ from the surface. Spin conditions: For 0.5 μm films: 10 s at a velocity of 5000 rpm (ramp = 1000 rpm/s), 10 min at V = 500 rpm (ramp = 500 rpm/s); 1.5 μm films: 10 s at a velocity of 1000 rpm (ramp = 100 rpm/s), 10 min at V = 500 rpm (ramp = 500 rpm/s); for 4.0 μm films: 10 s at a velocity of 450 rpm (ramp = 100 rpm/s), 10 min at V = 500 rpm (ramp = 500 rpm/s).

Polyviologen (PV) Cross-Linked Top-Layer Film Fabrication (6.0−11.3 μm). An amount of 75 mg of 2V-St·2OTs·2Cl cross-linker was weighed and added into a 10 mL round-bottom flask. Then 1.25 mg of lithium phenyl-2,4,6-trimethylbenzoylphosphinate (LAP) was added to the reaction flask. Then, 225 μL of methacrylic acid and 75 μL of deionized H_2O were added to the reaction flask for the 11.3 μm films. For the 6.0 μm films, an additional 75 μL of MeOH was added to the reaction flask to dilute the mixture. The mixture was sonicated to ensure that all cross-linker and initiator were dissolved. Then, the mixture was degassed through freeze−pump−thawing three times. The mixture was then transferred into a clean room and drop-cast on top of the polythiophene-coated substrate. The substrates were irradiated with a UV (365 nm) 75 W light source, positioned 3″ from the top of the film, for 6 h to ensure complete polymerization.

Electrochemistry

Linear sweep voltammetry (LSV) was conducted on both the PTh and PV only films as well as the bilayered film, all in a 0.1 M solution of $TBAPF_6$ in DMF. PTh solid-state LSV was obtained by dropping 5 μL of a 60 mg/mL solution of PTh in a 1:1 H_2O:MeOH mixture onto the surface of a glassy carbon electrode. The PV only films were formed following the procedure for the 1.5 μm film and were plated onto a cleaned ITO slide for use as the working electrode. The bilayered films were analyzed following the procedure for the 1.5 μm film and were plated onto a cleaned ITO slide for use as the working electrode. A Ag/AgCl reference in 1.0 M KCl in H_2O and platinum wire counter electrode were used.

UV−Vis Spectroscopy

UV−vis spectroscopy was recorded using an Agilent Cary 5000 spectrophotometer with a PbSmart NIR detector scanning from 200 to 1600 nm. All measurements were conducted in the solid state by aligning the respective films with the beam and scanning from 200 to 1600 nm.

Atomic Force Microscopy

Topographical data was collected from a Bruker Dimensions ICO atomic force microscope using a ScanAsyst-Air AFM tip with a scanning rate of 1 Hz. Various scanning windows were documented.

Profilometry

The thickness of the films was determined by making a thick scratch in the films with the back of a razor blade followed by obtaining topographical data from a KLA-Tencor Alpha-Step D-100 Profilometer. The thickness of the two individual layers was determined first by measuring the thickness of the polythiophene layer then the thickness of the bilayers. The thickness of the top layer could then be determined through subtraction.

Femtosecond Transient Absorption (fTA) Spectroscopy Information

fTA spectroscopy is a differential absorption (ΔAbs) measurement, where the broad, probe continuum is used to probe changes in the absorption spectra of the sample with and without excitation as a function of t after photoexcitation. For a single measurement at a given t, two transmission spectra of the probe laser are collected. One spectrum is the probe spectrum acquired with the excitation beam blocked. A second transmission probe spectrum is recorded with the excitation laser pulse traversing the sample at t before the probe pulse. The femtosecond TA experiments were performed using the output of a commercial Ti:sapphire amplifier laser system (800 nm, ∼2.3 W at 1 kHz, and ∼120 fs pulse width) and a commercial TA spectrometer. A fraction of the laser output was focused into a sapphire crystal to generate a white light continuum (450−760 nm) for use as the probe beam. The remainder of the laser output pumped a commercial optical parameter amplifier to provide excitation pulses at either 500 nm (2.48 eV) or 450 nm (2.76 eV) with a bandwidth of ∼12 nm. A motorized delay stage was used to control the delay time between the pump and probe pulses, t, with t < 1.5 ns. The data were collected for 2 s at each t. The unpolarized excitation and probe beams were gently focused on the sample, which was positioned orthogonally to the probe beam path. The excitation fluence was kept to ∼50 μJ cm^{-2} $pulse^{-1}$ to minimize multicarrier interactions and heating effects. A temporal resolution of ∼200 fs was achieved in these fTA measurements.

■ ASSOCIATED CONTENT

Supporting Information

The Supporting Information is available free of charge at https://pubs.acs.org/doi/10.1021/acspolymersau.1c00036.

> Synthesis and characterization of the respective monomer/cross-linker precursors to each functional polymer, as well as characterization data for each individual film and the bilayered films; more information related to femtosecond transient absorption spectroscopic measurements (PDF)

■ AUTHOR INFORMATION

Corresponding Author

Jonathan C. Barnes − *Department of Chemistry, One Brookings Drive, Washington University, St. Louis, Missouri 63130, United States;* orcid.org/0000-0003-2945-8691; Email: jcbarnes@wustl.edu

Authors

Mary K. Danielson − *Department of Chemistry, One Brookings Drive, Washington University, St. Louis, Missouri 63130, United States*

Jie Chen − *Department of Chemistry, One Brookings Drive, Washington University, St. Louis, Missouri 63130, United States;* orcid.org/0000-0002-6591-3412

Anna K. Vaclavek − *Department of Chemistry, One Brookings Drive, Washington University, St. Louis, Missouri 63130, United States*

Nathan D. Colley − *Department of Chemistry, One Brookings Drive, Washington University, St. Louis, Missouri 63130, United States*

Abdul-Haq Alli − *Department of Chemistry, One Brookings Drive, Washington University, St. Louis, Missouri 63130, United States*

Richard A. Loomis − *Department of Chemistry, One Brookings Drive, Washington University, St. Louis, Missouri 63130, United States;* orcid.org/0000-0002-3172-6336

Complete contact information is available at: https://pubs.acs.org/10.1021/acspolymersau.1c00036

Author Contributions

J.C.B. and M.K.D. conceived of the polythiophene and polyviologen bilayered film concept as a method of studying solid-state electron transfer. M.K.D., J.C., N.D.C., J.C.B., and R.A.L. designed the experiments. M.K.D., A.K.V., and A.-H.A. carried out all synthetic work. M.K.D. fabricated all films and acquired all CV data. M.K.D. and A.K.V. conducted all goniometry experiments. J.C. and R.A.L. performed all TA experiments.

Notes

The authors declare no competing financial interest.

■ ACKNOWLEDGMENTS

Funding support was provided by the David and Lucile Packard Foundation through J.C.B.'s Packard Fellowship for Science and Engineering. R.A.L. acknowledges support from NSF DMR-1905751. Mass spectrometry data was obtained using the NIH/NIGMS Biomedical Mass Spectrometry Resource at WUSTL (#8P41GM103422). The authors acknowledge financial support from Washington University in St. Louis and the Institute of Materials Science and Engineering for the use of instruments and staff assistance.

■ REFERENCES

(1) Helms, B. A.; Seferos, D. S. Virtual Issue: Designing Polymers for Use in Electrochemical Energy Storage Devices. *Macromolecules* **2019**, *52* (4), 1349−1353.
(2) Cheng, Y.-J.; Yang, S.-H.; Hsu, C.-S. Synthesis of Conjugated Polymers for Organic Solar Cell Applications. *Chem. Rev.* **2009**, *109* (11), 5868−5923.
(3) Cheng, P.; Li, G.; Zhan, X.; Yang, Y. Next-generation organic photovoltaics based on non-fullerene acceptors. *Nat. Photonics* **2018**, *12* (3), 131−142.
(4) Yu, J.; Zheng, Y.; Huang, J. Towards High Performance Organic Photovoltaic Cells: A Review of Recent Development in Organic Photovoltaics. *Polymers* **2014**, *6* (9), 2473−2509.
(5) Jensen, J.; Hösel, M.; Dyer, A. L.; Krebs, F. C. Development and Manufacture of Polymer-Based Electrochromic Devices. *Adv. Funct. Mater.* **2015**, *25* (14), 2073−2090.
(6) Marrocchi, A.; Lanari, D.; Facchetti, A.; Vaccaro, L. Poly(3-hexylthiophene): synthetic methodologies and properties in bulk heterojunction solar cells. *Energy Environ. Sci.* **2012**, *5* (9), 8457−8474.
(7) Gurney, R. S.; Lidzey, D. G.; Wang, T. A review of non-fullerene polymer solar cells: from device physics to morphology control. *Rep. Prog. Phys.* **2019**, *82* (3), 036601.
(8) Lee, C. W.; Kim, O. Y.; Lee, J. Y. Organic materials for organic electronic devices. *J. Ind. Eng. Chem.* **2014**, *20* (4), 1198−1208.
(9) Chen, W.; Zhang, Q. Recent progress in non-fullerene small molecule acceptors in organic solar cells (OSCs). *J. Mater. Chem. C* **2017**, *5* (6), 1275−1302.
(10) Gao, D.; Djukic, B.; Shi, W.; Bridges, C. R.; Kozycz, L. M.; Seferos, D. S. Evolution of the Electron Mobility in Polymer Solar Cells with Different Fullerene Acceptors. *ACS Appl. Mater. Interfaces* **2013**, *5* (16), 8038−8043.
(11) He, Y.; Chen, H.-Y.; Hou, J.; Li, Y. Indene-C60 Bisadduct: A New Acceptor for High-Performance Polymer Solar Cells. *J. Am. Chem. Soc.* **2010**, *132* (4), 1377−1382.
(12) Granqvist, C. G. Electrochromic tungsten oxide films: Review of progress 1993−1998. *Sol. Energy Mater. Sol. Cells* **2000**, *60* (3), 201−262.
(13) Sun, C.; Qin, S.; Wang, R.; Chen, S.; Pan, F.; Qiu, B.; Shang, Z.; Meng, L.; Zhang, C.; Xiao, M.; Yang, C.; Li, Y. High Efficiency Polymer Solar Cells with Efficient Hole Transfer at Zero Highest Occupied Molecular Orbital Offset between Methylated Polymer Donor and Brominated Acceptor. *J. Am. Chem. Soc.* **2020**, *142* (3), 1465−1474.
(14) Bird, C. L.; Kuhn, A. T. Electrochemistry of the viologens. *Chem. Soc. Rev.* **1981**, *10* (1), 49−82.
(15) Michaelis, L.; Hill, E. S. THE VIOLOGEN INDICATORS. *J. Gen. Physiol.* **1933**, *16* (6), 859−873.
(16) Hui, T.-W.; Baker, M. D. Redox Processes of Methyl Viologen Cation Radicals at Zeolite Y-Modified Electrodes. *J. Phys. Chem. B* **2002**, *106* (4), 827−832.
(17) Mayhew, S. G. The Redox Potential of Dithionite and SO-2 from Equilibrium Reactions with Flavodoxins, Methyl Viologen and Hydrogen plus Hydrogenase. *Eur. J. Biochem.* **1978**, *85* (2), 535−547.
(18) Prier, C. K.; Rankic, D. A.; MacMillan, D. W. C. Visible Light Photoredox Catalysis with Transition Metal Complexes: Applications in Organic Synthesis. *Chem. Rev.* **2013**, *113* (7), 5322−5363.
(19) Ko, H. C.; Park, S.-a.; Paik, W.-k.; Lee, H. Electrochemistry and electrochromism of the polythiophene derivative with viologen pendant. *Synth. Met.* **2002**, *132* (1), 15−20.
(20) Li, M.; Wei, Y.; Zheng, J.; Zhu, D.; Xu, C. Highly contrasted and stable electrochromic device based on well-matched viologen and triphenylamine. *Org. Electron.* **2014**, *15* (2), 428−434.
(21) Oh, H.; Seo, D. G.; Yun, T. Y.; Lee, S. B.; Moon, H. C. Novel viologen derivatives for electrochromic ion gels showing a green-colored state with improved stability. *Org. Electron.* **2017**, *51*, 490−495.
(22) Shah, K. W.; Wang, S.-X.; Soo, D. X.; Xu, J. Viologen-Based Electrochromic Materials: From Small Molecules, Polymers and Composites to Their Applications. *Polymers* **2019**, *11* (11), 1839.
(23) DiCarmine, P. M.; Schon, T. B.; McCormick, T. M.; Klein, P. P.; Seferos, D. S. Donor-Acceptor Polymers for Electrochemical Supercapacitors: Synthesis, Testing, and Theory. *J. Phys. Chem. C* **2014**, *118* (16), 8295−8307.
(24) Sathyamoorthi, S.; Kanagaraj, M.; Kathiresan, M.; Suryanarayanan, V.; Velayutham, D. Ethyl viologen dibromide as a novel dual redox shuttle for supercapacitors. *J. Mater. Chem. A* **2016**, *4* (12), 4562−4569.
(25) Ding, J.; Zheng, C.; Wang, L.; Lu, C.; Zhang, B.; Chen, Y.; Li, M.; Zhai, G.; Zhuang, X. Viologen-inspired functional materials: synthetic strategies and applications. *J. Mater. Chem. A* **2019**, *7* (41), 23337−23360.
(26) Hu, B.; Tang, Y.; Luo, J.; Grove, G.; Guo, Y.; Liu, T. L. Improved radical stability of viologen anolytes in aqueous organic redox flow batteries. *Chem. Commun.* **2018**, *54* (50), 6871−6874.
(27) Janoschka, T.; Martin, N.; Martin, U.; Friebe, C.; Morgenstern, S.; Hiller, H.; Hager, M. D.; Schubert, U. S. An aqueous, polymer-based redox-flow battery using non-corrosive, safe, and low-cost materials. *Nature* **2015**, *527* (7576), 78−81.
(28) Liu, T.; Wei, X.; Nie, Z.; Sprenkle, V.; Wang, W. A Total Organic Aqueous Redox Flow Battery Employing a Low Cost and Sustainable Methyl Viologen Anolyte and 4-HO-TEMPO Catholyte. *Adv. Energy Mater.* **2016**, *6* (3), 1501449.
(29) Martínez-González, E.; Flores-Leonar, M. M.; Amador-Bedolla, C.; Ugalde-Saldívar, V. M. Concentration Effects on the First Reduction Process of Methyl Viologens and Diquat Redox Flow Battery Electrolytes. *ACS Appl. Energy Mater.* **2021**, *4* (7), 6624−6634.
(30) Orgill, J. J.; Chen, C.; Schirmer, C. R.; Anderson, J. L.; Lewis, R. S. Prediction of methyl viologen redox states for biological applications. *Biochem. Eng. J.* **2015**, *94*, 15−21.
(31) Lin, Q.; Li, Q.; Batchelor-McAuley, C.; Compton, R. G. Use of 'split waves' for the measurement of electrocatalytic kinetics: methyl viologen mediated oxygen reduction on a boron-doped diamond electrode. *Phys. Chem. Chem. Phys.* **2013**, *15* (20), 7760−7767.
(32) Anandan, S. Viologen impregnated PVDF with TiO2 nanofiller as a solid polymer electrolyte for dye-sensitized solar cells. *Curr. Appl. Phys.* **2008**, *8* (1), 99−103.
(33) Sharma, G. D.; Sharma, S.; Roy, M. S. Electrical and photoelectrical properties of dye-sensitized allyl viologen-doped polypyrrole solar cells. *Sol. Energy Mater. Sol. Cells* **2003**, *80* (2), 131−142.
(34) Wang, Y.-F.; Wang, H.-Y.; Li, Z.-S.; Zhao, J.; Wang, L.; Chen, Q.-D.; Wang, W.-Q.; Sun, H.-B. Electron Extraction Dynamics in CdSe

and CdSe/CdS/ZnS Quantum Dots Adsorbed with Methyl Viologen. *J. Phys. Chem. C* **2014**, *118* (31), 17240−17246.
(35) Peterson, M. D.; Jensen, S. C.; Weinberg, D. J.; Weiss, E. A. Mechanisms for Adsorption of Methyl Viologen on CdS Quantum Dots. *ACS Nano* **2014**, *8* (3), 2826−2837.
(36) Amir, F.; Liles, K. P.; Delawder, A. O.; Colley, N. D.; Palmquist, M. S.; Linder, H. R.; Sell, S. A.; Barnes, J. C. Reversible Hydrogel Photopatterning: Spatial and Temporal Control over Gel Mechanical Properties Using Visible Light Photoredox Catalysis. *ACS Appl. Mater. Interfaces* **2019**, *11* (27), 24627−24638.
(37) Delawder, A. O.; Natraj, A.; Colley, N. D.; Saak, T.; Greene, A. F.; Barnes, J. C. Synthesis, self-assembly, and photomechanical actuator performance of a sequence-defined polyviologen crosslinker. *Supramol. Chem.* **2019**, *31* (8), 523−531.
(38) Greene, A. F.; Danielson, M. K.; Delawder, A. O.; Liles, K. P.; Li, X.; Natraj, A.; Wellen, A.; Barnes, J. C. Redox-Responsive Artificial Molecular Muscles: Reversible Radical-Based Self-Assembly for Actuating Hydrogels. *Chem. Mater.* **2017**, *29* (21), 9498−9508.
(39) Amir, F.; Li, X.; Gruschka, M. C.; Colley, N. D.; Li, L.; Li, R.; Linder, H. R.; Sell, S. A.; Barnes, J. C. Dynamic, multimodal hydrogel actuators using porphyrin-based visible light photoredox catalysis in a thermoresponsive polymer network. *Chem. Sci.* **2020**, *11* (40), 10910−10920.
(40) Liles, K. P.; Greene, A. F.; Danielson, M. K.; Colley, N. D.; Wellen, A.; Fisher, J. M.; Barnes, J. C. Photoredox-Based Actuation of an Artificial Molecular Muscle. *Macromol. Rapid Commun.* **2018**, *39* (17), 1700781.
(41) Shah, K. W.; Wang, S.-X.; Soo, D. X. Y.; Xu, J. Viologen-Based Electrochromic Materials: From Small Molecules, Polymers and Composites to Their Applications. *Polymers* **2019**, *11* (11), 1839.
(42) Shu, C.-F.; Wrighton, M. S. Synthesis and Electrochemical Properties of a Polythiophene—Viologen Polymer. In *Electrochemical Surface Science*; American Chemical Society: 1988; Vol. *378*, pp 408−430.
(43) Xing, C.; Xu, Q.; Tang, H.; Liu, L.; Wang, S. Conjugated Polymer/Porphyrin Complexes for Efficient Energy Transfer and Improving Light-Activated Antibacterial Activity. *J. Am. Chem. Soc.* **2009**, *131* (36), 13117−13124.
(44) Adeniyi, A. A.; Ngake, T. L.; Conradie, J. Cyclic Voltammetric Study of 2-Hydroxybenzophenone (HBP) Derivatives and the Correspondent Change in the Orbital Energy Levels in Different Solvents. *Electroanalysis* **2020**, *32* (12), 2659−2668.
(45) Liu, J.; Chen, S.; Qian, D.; Gautam, B.; Yang, G.; Zhao, J.; Bergqvist, J.; Zhang, F.; Ma, W.; Ade, H.; Inganäs, O.; Gundogdu, K.; Gao, F.; Yan, H. Fast charge separation in a non-fullerene organic solar cell with a small driving force. *Nat. Energy* **2016**, *1* (7), 16089.
(46) Swamy, N. K. S. S.; Santhosh, A. S. Conductive Polymers and their Nanohybrid Transducers for Electrochemical Biosensors Applications: A Brief Review. *Indian J. Adv. Chem. Sci.* **2017**, *S2*, 6−9.
(47) Pande, G. K.; Kim, N.; Choi, J. H.; Balamurugan, G.; Moon, H. C.; Park, J. S. Effects of counter ions on electrochromic behaviors of asymmetrically substituted viologens. *Sol. Energy Mater. Sol. Cells* **2019**, *197*, 25−31.
(48) Ionescu, A.; Cornut, D.; Soriano, S.; Guissart, C.; Van Antwerpen, P.; Jabin, I. Efficient 'one-pot' methodology for the synthesis of novel tetrahydro-*β*-carboline, tetrahydroisoquinoline and tetrahydrothienopyridine derivatives. *Tetrahedron Lett.* **2013**, *54* (45), 6087−6089.

https://doi.org/10.1021/acspolymersau.1c00036
ACS Polym. Au 2022, 2, 118−128